Angular normalized glandular dose coefficient in breast CT: clinical data study

Hsin Wu Tseng, Andrew Karellas, Srinivasan Vedantham*
Department of Medical Imaging, The University of Arizona,
1501 N Campbell Ave., Tucson, AZ, USA 85724

ABSTRACT

The goal of this study is to understand how the normalized glandular dose coefficient (DgN^{CT}) varies with projection angle in dedicated cone-beam breast computed tomography (CBBCT). Seventy-five CBBCT clinical datasets from a research database were used for this study. All samples were segmented into skin, adipose and fibroglandular tissues. The segmented volumes were used in a Monte Carlo simulation package (GATE 8.0) to estimate the radiation dose at 10 angles in a full scan. An analytical model is proposed, and this model predicted that the angular DgN^{CT} follows a sine wave and the maximum is related to the center of geometry of the fibroglandular tissue ($\mathrm{COG_f}$). The angular DgN^{CT} from Monte Carlo simulations was consistent with our model and follows a sine wave with amplitude of 0.0376. The maximum of the wave occurs when the x-ray source is approximately at head position, which is consistent with our model. Our results indicate that the higher angular DgN^{CT} occurs when the x-ray source is superior to the breast. This suggests using a x-ray source trajectory inferior to the breast for short-scan CBBCT design.

Keywords: breast CT, mean glandular dose, Monte Carlo, radiation dose

1. INTRODUCTION

The mean glandular dose in cone-beam breast CT (CBBCT) can be estimated by the product of normalized glandular dose (DgN^{CT}) coefficient and the air kerma (*AK*) measured at the axis of rotation (AOR) without any object. Monte Carlo (MC) simulations are the most common method to compute the energy deposited in the fibroglandular tissues [1]–[8]. The DgN^{CT} depends on the x-ray spectrum and the breast model. The semi-ellipsoidal breast model with a homogeneous distribution of fibroglandular tissue [7], [9], [10] and patient-specific breast model [6], [7] are the two common models used in CBBCT studies. The former model uses the effective chest-wall diameter (D_{eff}), the chest wall-to-nipple length (*CNL*), and fibroglandular fraction (f_g) of the breast to create a semi-ellipsoidal model, and every voxel, except the skin, has the same f_g. The second model segments each 3D reconstructed breast volume into skin, adipose, and fibroglandular tissues, in addition to air. The homogeneous semi-ellipsoidal model was found to overestimate DgN^{CT} because this model overestimates the amount of the fibroglandular tissue along the periphery of the breast. Since the DgN^{CT} homogeneous semi-ellipsoidal model can be described by a fitting function [11], here we focus on the patient-specific model in this study.

To our best knowledge, studies in literature only considered DgN^{CT}, but none have considered the variation of the DgN^{CT} with the projection angles, i.e., angular DgN^{CT}. We are particularly interested in DgN^{CT} because we have developed feasible image reconstruction algorithms for short-scan and sparse-view acquisitions [12], [13], and we would like to understand which angular range should be used for short-scan acquisition to reduce the radiation to the breast either for prone or upright patient-position CBBCT systems.

A cohort of 75 CBBCT datasets from a research database of subjects who had participated in a prior IRB-approved clinical trial was used in this study. A validated MC simulation code in our recent publication [10] and following the guideline of the Task Group No. 268 of the American Association of Physics in Medicine (AAPM)[14] was used here to compute the angular DgN^{CT}.

*svedantham@arizona.edu

7th International Conference on Image Formation in X-Ray Computed Tomography,
edited by Joseph Webster Stayman, Proc. of SPIE Vol. 12304, 123040Q
 · 0277-786X · doi: 10.1117/12.2646683

2. MATERIALS AND METHODS

2.1 CBBCT system

The projections were acquired by a CBBCT system that is a Pre-FDA approval prototype (KBCT1000, Koning Corp., West Henrietta, NY). The operated x-ray tube was RAD71-SP (Varex Imaging, Salt Lake City, UT), and the x-ray was operated at 49 kV with a pulse-width of 8 milliseconds. 300 projections with uniform 1.2 deg/view angular sampling in a full scan (360 deg) were performed. A CsI:Tl scintillator coupled, amorphous silicon-based flat-panel detector (PaxScan 4030CB, Varex Imaging, Salt Lake City, UT) used in the CBBCT system. The operating pixel size of this detector is 0.388 mm, and the dimension of the detector is 1024×768. The distance between the source and the AOR is 650 mm, and the source-to-detector distance is 898 mm.

2.2 Angular DgN^{CT} computation

The breast images were all first reconstructed by our developed deep learning-based algorithm, multi-slice residual dense network (MS-RDN) [13], that reduces image noise. Then all MS-RDN reconstructed images were segmented into air, skin, adipose, and fibroglandular tissues (Fig. 1) using a previously reported method [15]. The *CNL*, D_{eff}, and f_g can be estimated from segmented images for a semi-ellipsoidal homogeneous breast model.

The DgN^{CT} (mGy/mGy) of the patient-specific breast model can be calculated as [5], [6]

$$\mathrm{DgN}_{\mathrm{hete}}^{\mathrm{CT}} = \frac{\mathrm{E_{g,dep}}}{\mathrm{n_g m_g \times AK(E)}} \tag{1}$$

where the subscript, *hete* represents heterogeneous tissue distribution, $\mathrm{E_{g,dep}}$ is the total energy deposited in all fibroglandular tissue voxels, $\mathrm{n_g}$ indicates the total number of fibroglandular tissue voxels, $\mathrm{m_g}$ is the mass of a fibroglandular tissue voxel, and $AK(E)$ is the air kerma at the breast center with the energy, *E*, of the incident photons. The same computational method was used for calculating the angular DgN^{CT}. In MC simulations, all photons were radiated to the breast from the assigned x-ray source position (angle). The MC simulations were performed using the MC code (GATE 8.0) validated in our previous study [10]. The number of photons was 10^6 as suggested by literature [7], [16], and resulted in a variation of less than 0.7%.

The angular DgN^{CT} of the homogeneous breast of a semi-elliptical shape is the same as its DgN^{CT} at any angle because of the rotational symmetry. The angular DgN^{CT} of this model can be expressed as a fitting function (standard deviation is 1.13%) [11]

$$\begin{aligned} DgN_{Fit}^{CT} = &\left[1.0758247 - 0.2353669 \times \ln\left(D_{eff}\right) - 0.1253462 f_g\right] \\ &\times \left[0.1153 \times \ln\left(\frac{CNL}{D_{eff}}\right) + 1.0818\right] \end{aligned} \tag{2}$$

2.3 Simplified Math Model

The angular DgN^{CT} in Eq. (1) is related to the energy deposited on the fibroglandular tissues, which is proportional to the pathlengths (PL) of photons through the fibroglandular tissues. To easily demonstrate this concept, a 2D circle of a finite size presents the fibroglandular tissues here. The center of the circle is the center of the geometry of the fibroglandular tissues ($\mathrm{COG_f}$). The PL can be analytically solved as

$$PL = 2\left\{\begin{matrix} \frac{(L+R\cos\beta)^2(1+\tan\alpha\tan(\alpha+\theta))^2}{1+tan^2(\alpha+\theta)} \\ +r^2 - (L+R\cos\beta)^2(1+tan^2\alpha) \end{matrix}\right\}^{1/2} \tag{3}$$

where L, R, r, and β, α, and θ are the distance between the x-ray source and AOR, the radius of the orbit of the 2D circle, the radius of the circle, the polar angle of the circle in the orbit, the angle between the central line of the circle and the central line of the fan-beam, the angle deviated from the central line of the circular object, respectively. The figure is depicted in Fig. 2. Similar to the concept of the *Radon* transform, the curve of the PL is a sine wave varying with projection angle.

3. RESULTS

3.1 Total Simulation Time

All MC simulations were performed on a Dell workstation 7810 with Intel Xeon CPU (3.20 GHz) and 32 GB RAM. For each angle, the MC simulation took approximately 40 minutes, resulting in 40×10×75=30000 minutes for all 75 samples.

3.2 Numerical results of the simplified math model

Numerical results of two particular examples of our simplified math model are when the $\mathrm{COG_f}$ is located at the center and above the AOR (i.e. β=0 in Eq. (3) and Fig. 2). Let the radius of the $\mathrm{COG_f}$ be 15 mm with (1) 0 mm (reference) and (2) 50 mm distance away from the AOR. Without losing any generality, $\theta = 1^{\circ}$ (or -1°) was considered here. The results (Fig. 3) show that the PL is a sine wave as predicted and in this particular example, the minimum of the curve occurs when the x-ray source is at ϕ=180 deg (feet position). The average PL of the sine wave is 0.1296 *mm* less than the reference. The sine wave has the same PL as that of the reference at ϕ=92.2042 deg and 267.7958 deg, which can be analytically solved by Eq. (3).

3.3 Center of the geometry of fibroglandular tissues

In MC simulations, the center of the geometry of the entire breast $\mathrm{COG_b}$ is at the AOR. The deviation of $\mathrm{COG_f}$ from $\mathrm{COG_b}$ for each sample was shown in Fig. 4. The breast laterality is factored with 90 deg representing medial and 270 deg representing lateral aspects of the breast. It was found that 62.67% of samples have $\mathrm{COG_f}$ between 36 deg and 324 deg. From the previous section, the numerical results show that the minimum of the PL curve would happen at 180 deg if the $\mathrm{COG_f}$ is exactly at 0 deg. Thus, the angular DgN^{CT} in this particular dataset should be a sine wave with a minimum at approximately within the range of 144 to 216 deg.

3.4 Angular DgN^{CT}

For each breast volume, the angular DgN^{CT} was normalized by the DgN^{CT} from the homogeneous semi-ellipsoidal model (reference) to characterize its deviation. The average of this normalized angular DgN^{CT} from the 75 breast CT volumes is shown in Fig. 5. Consistent with the prediction from section III. B and III. C above, the curve of the angular DgN^{CT} is approximately a sine wave with a minimum between 144 deg and 216 deg. The curve can be fitted to sine wave of the form $0.0376\sin(\emptyset + 83^{\circ})$, with a root mean square error of 0.0106.

4. DISCUSSION AND CONCLUSIONS

In this study, we have investigated the variation in $\mathrm{DgN^{CT}}$ with x-ray projection angle for real breasts using both numerical study of PL calculation and using MC simulations. Although the PL calculation is based on the 2D geometry, it provides us an easy way to understand how the DgN^{CT} changes when a real 3D breast is scanned in the CBBCT system. The MC results were consistent with our simplified math model and $\mathrm{COG_f}$ analysis. As predicted by our theory, there is higher energy deposition in most of the patients' breasts when the x-ray source is approximately superior to the breast, i.e., between the shoulders and above the breast. Thus, to reduce the radiation dose to the patients in short-scan CBBCT acquisition, it is preferable to avoid acquiring projections superior to the breast. This implies an x-ray source trajectory that is inferior to the breast. Further, this design would allow the detector to traverse below the chin, which could avoid the neck strain reported in a prior study [17] due to the need to turn the patient's head to accommodate the x-ray source trajectory. Development of such an upright CBBCT system is in progress. The determination of the angular sampling interval for the short-scan acquisition should depend on the design and the implementation of the image reconstruction algorithms.

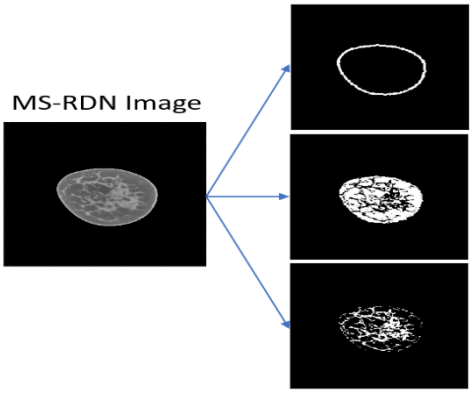

Figure 1. Segmentation of the image. The images were reconstructed by MS-RDN deep learning algorithm. Each image was then segmented into air, skin, adipose, and fibroglandular tissues.

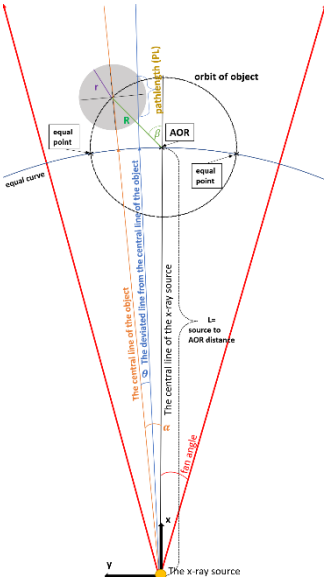

Figure 2. Simplified mathematical model. A 2D circular object in a fan-beam geometry.

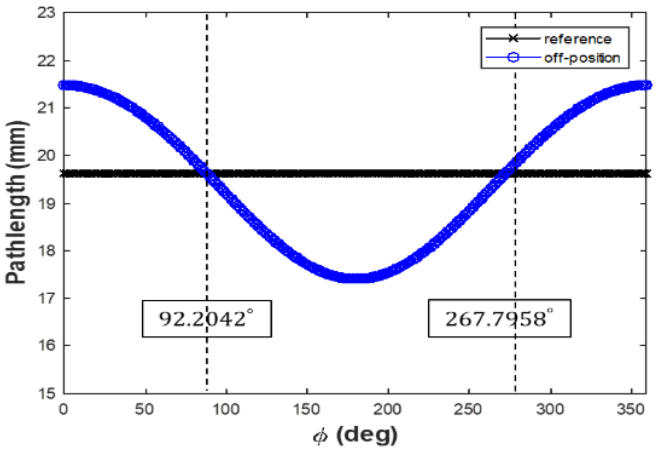

Figure 3. The pathlength of the object off positioned above from the AOR. ϕ is the angle of the x-ray source.

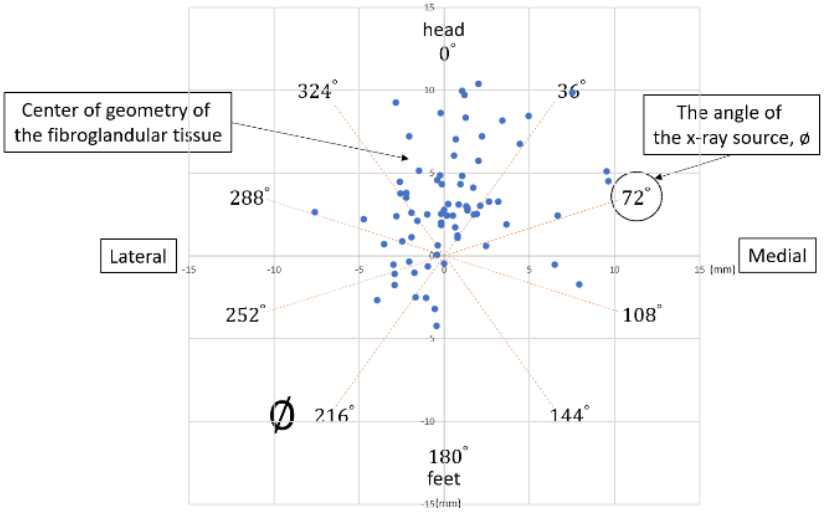

Figure 4. Center of the geometry of the fibroglandular tissues (COG_f) deviated from the center of the geometry of the entire breast (COG_b). ϕ is the angle of the x-ray source.

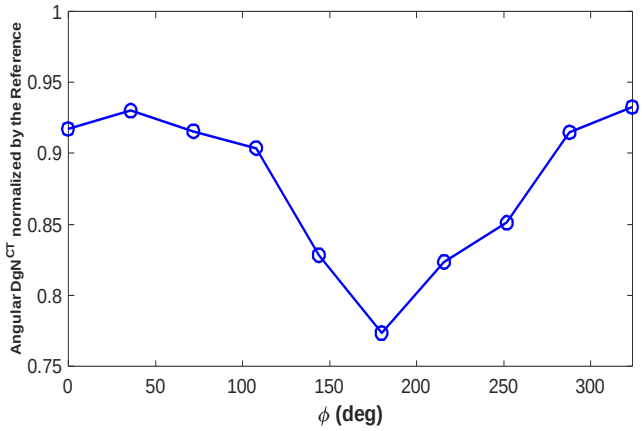

Figure 5. The angular DgN^{CT} of the patient-specific model is normalized by the reference (homogeneous breast of semi-elliptical shape).

REFERENCES

[1] Boone, J. M., "Glandular breast dose for monoenergetic and high-energy X-ray beams: Monte Carlo assessment," Radiology, 213(1), 23–37 (1999).

[2] Boone, J. M., Shah, N., and Nelson, T. R., "A comprehensive analysis of DgN(CT) coefficients for pendant-geometry cone-beam breast computed tomography," Med Phys, 31(2), 226–235 (2004).

[3] Boone, J. M., "Normalized glandular dose (DgN) coefficients for arbitrary X-ray spectra in mammography: computer-fit values of Monte Carlo derived data," Med Phys, 29(5), 869–875 (2002).

[4] Dance, D. R., "Monte Carlo calculation of conversion factors for the estimation of mean glandular breast dose," Phys Med Biol, 35(9), 1211–1219 (1990).

[5] Hernandez, A. M., Becker, A. E., and Boone, J. M., "Updated breast CT dose coefficients (DgNCT) using patient-derived breast shapes and heterogeneous fibroglandular distributions," Med Phys, 46(3), 1455–1466 (2019).

[6] Sarno, A., Dance, D. R., van Engen, R. E., Young, K. C., Russo, P., Di Lillo, F., Mettivier, G., Bliznakova, K., Fei, B., and Sechopoulos, I., "A Monte Carlo model for mean glandular dose evaluation in spot compression mammography," Med Phys, 44(7), 3848–3860 (2017).

[7] Sechopoulos, I., Feng, S. S. J., and D'Orsi, C. J., "Dosimetric characterization of a dedicated breast computed tomography clinical prototype," Med Phys, 37(8), 4110–4120 (2010).
[8] Sechopoulos, I., Sabol, J. M., Berglund, J., Bolch, W. E., Brateman, L., Christodoulou, E., Flynn, M., Geiser, W., Goodsitt, M., Jones, A. K., Lo, J. Y., Maidment, A. D. A., Nishino, K., Nosratieh, A., Ren, B., Segars, W. P., and Von Tiedemann, M., "Radiation dosimetry in digital breast tomosynthesis: report of AAPM Tomosynthesis Subcommittee Task Group 223," Med Phys, 41(9), 091501 (2014).
[9] Thacker, S. C. and Glick, S. J., "Normalized glandular dose (DgN) coefficients for flat-panel CT breast imaging," Phys Med Biol, 49(24), 5433–5444 (2004).
[10] Tseng, H. W., Karellas, A., and Vedantham, S., "Radiation dosimetry of a clinical prototype dedicated cone-beam breast CT system with offset detector," Med Phys, 48(3), 1079–1088 (2021).
[11] Vedantham, S., Shi, L., Karellas, A., O'Connell, A. M., and Conover, D. L., "Personalized estimates of radiation dose from dedicated breast CT in a diagnostic population and comparison with diagnostic mammography," Phys. Med. Biol., 58(22), 7921–7936 (2013).
[12] Tseng, H. W., Karellas, A., and Vedantham, S., "Sparse-view, short-scan, dedicated cone-beam breast computed tomography: image quality assessment," Biomed Phys Eng Express (2020).
[13] Fu, Z., Tseng, H. W., Vedantham, S., Karellas, A., and Bilgin, A., "A residual dense network assisted sparse view reconstruction for breast computed tomography," Sci Rep, 10, 21111 (2020).
[14] Sechopoulos, I., Rogers, D. W. O., Bazalova-Carter, M., Bolch, W. E., Heath, E. C., McNitt-Gray, M. F., Sempau, J., and Williamson, J. F., "RECORDS: improved Reporting of montE CarlO RaDiation transport Studies: Report of the AAPM Research Committee Task Group 268," Med Phys, 45(1), e1–e5 (2018).
[15] Vedantham, S., Shi, L., Karellas, A., and O'Connell, A. M., "Dedicated breast CT: Fibroglandular volume measurements in a diagnostic population," Med Phys, 39(12), 7317–7328 (2012).
[16] Vedantham, S., Shi, L., Karellas, A., and Noo, F., "Dedicated breast CT: radiation dose for circle-plus-line trajectory," Med Phys, 39(3), 1530–1541 (2012).
[17] O'Connell, A., Conover, D. L., Zhang, Y., Seifert, P., Logan-Young, W., Lin, C.-F. L., Sahler, L., and Ning, R., "Cone-Beam CT for Breast Imaging: Radiation Dose, Breast Coverage, and Image Quality," American Journal of Roentgenology, 195(2), 496–509 (2010).